Clumps With Self Contained Magnetic Field And Their Interaction With Shocks

Shule Li

Adam Frank and Eric Blackman

Department of Physics and Astronomy, University of Rochester, Rochester, NY, 14627

shuleli@pas.rochester.edu

Received __________________; accepted __________________

ABSTRACT

Problems involving magnetized clouds and clumps, especially their interaction with shocks are common in astrophysical environments and have been a topic of research in the past decade. Many previous numerical studies have focused on the problem of clumps immersed in a globally uniform magnetic field subject to a oncoming shock. However, realistic clumps may have tangled magnetic field self contained within them. This magnetic field will be compressed by the shock and its energy spectrum and spatial structure may affect the evolution of the clump during the shock encounter. Using our parallel MHD code AstroBEAR, we set up a series of initial state with magnetized clumps of different contained magnetic field configurations, study their interaction with shocks, and compare them to the previous studied global uniform field scenario. We demonstrate through the discussion that the self contained magnetic field can render a more complicated post shock behavior for the clumps, however, the evolution of such scenario is still governed by various physics time scale conceivable from the initial setup.

Subject headings: magneto-hydrodynamics, planetary nebula, radiative shocks, MHD clumps, MHD jets

1. Introduction

2. MHD Equations with Radiative Cooling

The simulations are done using parallel MHD code AstroBEAR developped by Adam Frank's group at the University of Rochester. It is a powerful tool to solve MHD equations with radiative cooling:

$$\frac{\partial \rho}{\partial t} + \nabla \cdot (\rho \mathbf{v}) = \mathbf{0}, \tag{1}$$

$$\frac{\partial (\rho \mathbf{v})}{\partial t} + \nabla \cdot [\rho \mathbf{v}\mathbf{v} + (p + \frac{B^2}{8\pi})\mathbf{I} - \frac{\mathbf{B}\mathbf{B}}{4\pi}] = 0, \tag{2}$$

$$\frac{\partial \mathbf{B}}{\partial t} + \nabla \times (\mathbf{v} \times \mathbf{B}) = 0, \tag{3}$$

$$\frac{\partial E}{\partial t} + \nabla \cdot [\mathbf{v}(E + p + \frac{B^2}{8\pi}) - \frac{\mathbf{B}(\mathbf{B} \cdot \mathbf{v})}{8\pi}] - \Lambda(n, T) = 0, \tag{4}$$

where ρ, n, $\mathbf{v}$, $\mathbf{B}$ and p are the density, particle number density, velocity, magnetic field, and pressure, and E denotes the total energy given by

$$E = \epsilon + p\frac{\mathbf{v} \cdot \mathbf{v}}{2} + \frac{\mathbf{B} \cdot \mathbf{B}}{8\pi}, \tag{5}$$

where the internal energy ϵ is given by

$$\epsilon = \frac{p}{\gamma - 1} \tag{6}$$

and $\gamma = 5/3$. We denote the radiative cooling by a function of number density and temperature: Λ. In our simulations, we implement the Dalgarno McCray cooling table as it is more realistic comparing to simple analytic cooling functions (Dalgarno & McCray (1972)).

The above MHD equations are solved with the MUSCL (Monotone Upstream-centered Schemes for Conservation Laws) primitive method with TVD (Total Variation Diminishing) preserving Runge-Kutta temporal interpolation. The resistivity is ignored in our calculation so that the dissipation of the magnetic field is numerical only. Small artificial viscosity and diffusion are implemented in order to achieve required stability and symmetry. AstroBEAR has shown good scaling on more than thousands of processors, the simulations presented in this paper are done on 1024 cores on IBM Bluegene type machine.

3. Problem Description and Simlation Setup

The series of simulations presented in this paper are based on initial conditions with the same clump, ambient and shock conditions only with different initial magnetic field setup. The initial condition is illustrated by the following figure. The domain is a box with dimensions $2400a.u. \times 60a.u. \times 60a.u.$, and open boundary conditions on the six sides of the box.

EDITOR: PLACE FIGURE 1 HERE.

The ambient gas is non-magnetized and isothermal, with a particle number density of $1cc^{-1}$ and temperature of 10^4 K. A clump with radius of $r_c = 150a.u.$ is in thermal pressure equilibrium with the ambient medium. The clump has a density contrast of $\chi = 100$, i.e., particle number density of $100cc^{-1}$ and a temperature of 100 K . It also contains an internal magnetic field with a peak magnetic induction of $30.88\mu G$. We define β_{min} and β_{avg} as the minimum ratio of thermal pressure to magnetic pressure and the ratio of thermal pressure to averaged magnetic pressure inside the clump, respectively:

$$\beta_{min} = \frac{P_{thermal}}{P_{B,peak}} \tag{7}$$

$$\beta_{avg} = \frac{P_{thermal}}{P_{B,avg}} \tag{8}$$

where $P_{B,peak}$ and $P_{B,avg}$ denote the peak and average magnetic field pressure respectively. In our simulations, we focus on the cases when the contained magnetic field is either purely poloidal or purely toroidal. Since poloidal and toroidal field configurations are different, the same peak magnetic pressure may yield different average magnetic field pressure. For the toroidal only field configuration, the peak magnetic induction of $30.88\mu G$ gives a β_{min} of 0.036 and a β_{avg} of 0.1. For the poloidal only field configuration, the same peak magnetic induction gives the same β_{min} but a β_{avg} of 1. The small value of β indicates that the clump is magnetic dominated. Since the magnetic field contained is not in a force free state, the clump will be deformed by the contained field at the time scale of:

$$\tau_{mag} = \frac{r_c}{u_{Alfven}} \approx 276yrs \tag{9}$$

where u_{Alfven} is the Alfven speed of the contained field calculated from the average magnetic energy density inside the clump.

The incoming shock has a temperature of 10^6 K and Mach number 10 (ratio between the speed of the shock and the ambient sound speed). We identify the clump crushing time scale as:

$$\tau_{cc} = \frac{\sqrt{\chi} r_c}{u_{wind}} \approx 95yrs \tag{10}$$

The shock temperature is chosen so that the cooling time scale for the bow shock τ_{bow} is well below the clump crushing time to ensure effective cooling:

$$\tau_{bow} \approx 48yrs \ll \tau_{cc} \tag{11}$$

We also define the σ parameters of the shock: $\sigma_{thermal} = K_{shock}/E_{thermal}$ and $\sigma_{mag} = K_{shock}/E_{mag}$ as the ratio between the kinetic energy density of the shock and the thermal or average magnetic energy density contained in the clump, respectively. From previously given parameters, we can determine that $\sigma_{thermal} \approx 222$ and $\sigma_{mag} \approx 33$. Therefore, although the clump is magnetic dominated, the shock is much more energetic than either thermal or magnetic energy contained inside the clump. We run the simulation from time $t = 0$ to time $t \approx 333 yrs$, i.e. $3.5\tau_{cc}$. We will use the clump crushing time τ_{cc} as our unit of time throughout the rest of the paper.

We study the situation when the clump contains an ordered magnetic field by running the simulations described in the following table:

EDITOR: PLACE TABLE 1 HERE.

The field configurations are illustrated in the following diagram:

EDITOR: PLACE FIGURE 3 HERE.

4. Simulation Results

Figure 03 shows the result of simulation with shocked clump when the internal magnetic field is a toroidal field oriented aligned with the shock propagation direction (coded TA in the previous section). Panels (a), (b), (c) correspond to different evolution time: τ_{cc}, $2\tau_{cc}$ and $3.5\tau_{cc}$. For the toroidal field aligned with the shock, the morphology evolution of the clump is similar to that of the non magnetized case. But at $2\tau_{cc}$, instead of being eroded by the RT instability and expand, the clump material continues to collpase towards the symmetry axis due to the pinching of the toroidal magnetic field. Because of the continuation of compress, the boundary flows of the clump does not fill the downstream and form a large volume of turbulence but rather being concentrated into a cone shaped space. At $3.5\tau_{cc}$, the clump material is compressed into a shaft shaped cone with the toroidal field tightly wrapping around it. This geometry prevents the clump material from mixing with the wind, and confines the downstream flow into a much smaller volume comparing to the non magnetized case. The final snapshot resembles a "nose cone" observed in the MHD jet simulations, with a small Mach angle.

EDITOR: PLACE FIGURE 4 HERE.

Figure 04 shows a simulation using the same setup as above, only with the axis of toroidal field perpendicular to the shock (coded TP previously). We can immediately see differences in terms of clump material morphology comparing the first panel of Figure 03. In this case, the field wants to pinch the clump onto its axis (z axis by definition), but the shock wants to compress the clump onto x axis. The result is a difference in the aerodynamical resistance to the shock compression: the magnetized clump is harder to compress along z axis than x axis. As a result, the clump becomes football shaped at τ_{cc}. The prolonged clump continues to be eroded by the incoming shock, at $2\tau_{cc}$, the clump begins to fragment mostly along the z axis because of the lack of compression by shock or field pinch. We can see the clump surface is protected better than the clump center: there is a partial ring shaped feature at the center of the clump. This is because the surface has a stronger field concentration compared to the center in the case of toroidal configuration. At the end of the simulation, the clump gets further fragmented along z axis as a result of instability erosion and cooling, forming a spread of cold, magnetized "clumplets".

EDITOR: PLACE FIGURE 5 HERE.

Figure 05 shows the simulation of shocked clump when the internal field is poloidal and oriented along the shock direction (coded PA). In this case, there is a strong field concentration at the clump axis, as well as a relatively weak field concentration at the clump surface. When the axis is aligned with the shock, we can see that during the compression phase, at τ_{cc}, the clump is compressed radially similar to the non magnetized case, with a flatter head. Then, at $2\tau_{cc}$, we again see different feature comparing to the previous studied cases. Here, the clump expands as in the non magnetized case, but it also develops a "shaft" shaped core, corresponding to the region with strong field concentration. We see that those regions with small initial field concentration get pushed and compressed into those regions with a higher initial field concentration (clump axis and surface) by the shock. The "shaft" feature has a relatively low β comparing to the rest of the clump. It gradually deforms as a result of field pinching (pointing outwards from the axis) at the time scale of τ_{mag}, which is about $2.8\tau_{cc}$. Consequently, at $3.5\tau_{cc}$, the "shaft" disappears and the clump is fragmented into an array of cold, magnetized "clumplets", similar to the TP case. The difference is that, in the PA case, the clumplets are distributed on a circle, corresponding to the location of initial clump surface.

EDITOR: PLACE FIGURE 6 HERE.

Figure 06 shows the simulation similar to the previous one, only with the axis of the poloidal field oriented perpendicular to the shock direction (PP). In this case, we also observe a compression phase similar to the non manetized case with a flatter clump head. But the influence of different field orientation is evident at $2\tau_{cc}$. Here, the field concentration also leads to a "shaft" and a "ring" shape as in the PA case, but both the "ring" and the "shaft" are partially eroded by the incoming shock. The "shaft" is then fragmented by the shock rather than the field pinch, and the "ring" leaves a horse hoof shaped structure because the shock is coming from the sideway. As a result, two large "clumplets" located on the y-z plane, are formed at $3.5\tau_{cc}$. Notice that the previously mentioned four different cases all have their unique downstream features. In the TA case, the material is mostly compressed into a cone, leading to very limited downstream turbulent region. In both TP and PP cases, the turbulence fills a much larger region, but still does not fill the entire box downstream. In the PA case, because of the expanding "ring" feature, the downstream turbulence fills the entire box at downstream. We will see the implecation of the different turbulence feature in these cases when discussing the evolution of various physics quantities in the next section.

EDITOR: PLACE FIGURE 7 HERE.

To illustrate the postshock distribution of magnetic field, we plot the density and field pressure by cutting through the center of the simulation box in figure 07. It shows that the field follows the clump material distribution, as is expected in our simulations where the diffusion processes are all numerical only. Notice the field distribution in the two toroidal cases has a further "reach" comparing to the two poloidal cases. This is resulted from different initial β_{avg}: the two toroidal cases contain more magnetic energy initially comparing to the poloidal cases.

EDITOR: PLACE FIGURE 8 HERE.

5. Discussion

6. Conclusion and Acknowledgements

REFERENCES

Dalgano, A., & McCray, R.A. 1972, ARA&A, 10, 375

Jones, T.W., Ryu, Dongsu, & Tregillis, I.L. 1996, ApJ, 473, 365

This manuscript was prepared with the AAS LaTeX macros v5.2.

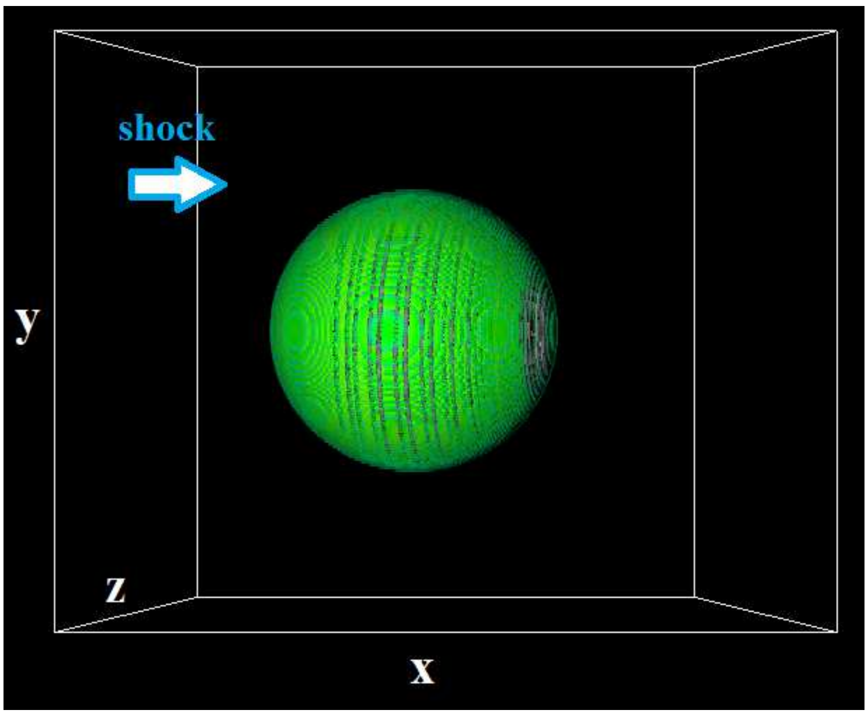

Fig. 1.— The initial setup of the clump simulations. The actual domain is four times as long on x as on y and z. The upcoming planar shock is at the left edge of the domain, propagating rightward along the x axis. The stripes on the clump surface denote a contained toroidal magnetic field with its axis aligned with x axis inside the clump.

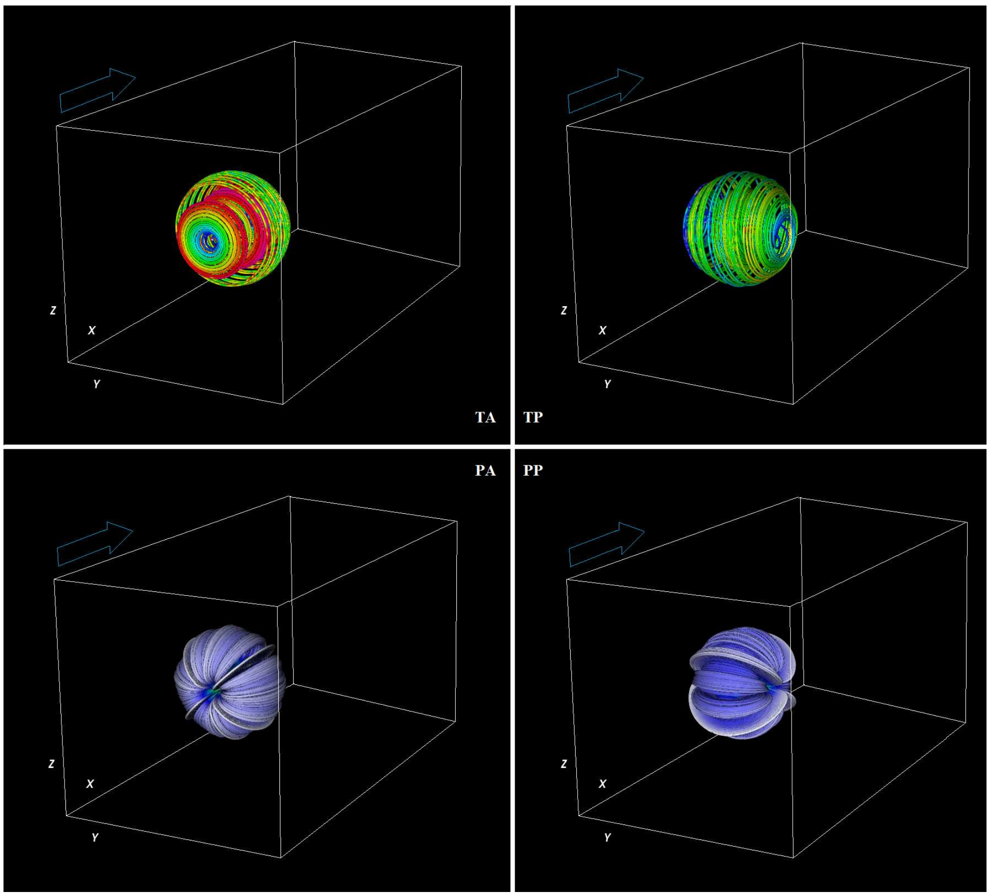

Fig. 2.— The initial setup of the clump magnetic field. The actual domain is four times as long on x as on y and z. The first letter denotes the field configuration: T for toroidal only; P for poloidal only. The second letter denotes the field orientation with respect to the shock propagation direction: A for aligned; P for perpendicular. The blue arrow denotes the shock direction.

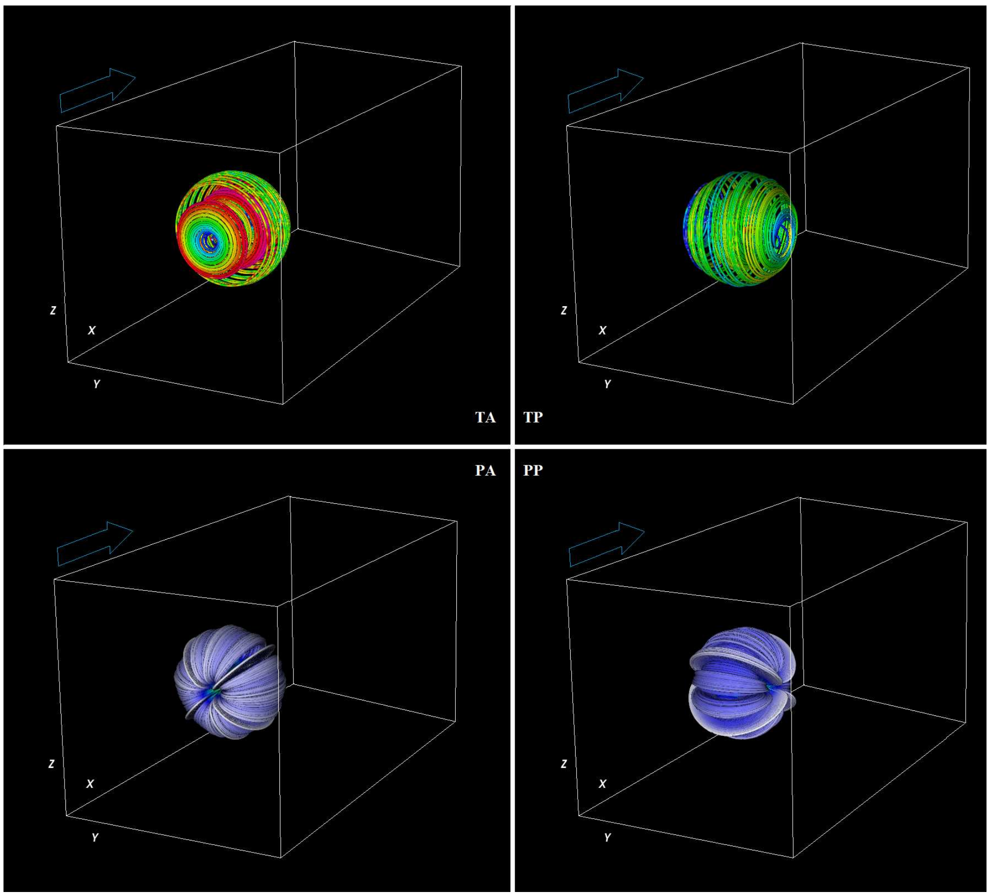

Fig. 3.— The initial setup of the clump magnetic field. The actual domain is four times as long on x as on y and z. The first letter denotes the field configuration: T for toroidal only; P for poloidal only. The second letter denotes the field orientation with respect to the shock propagation direction: A for aligned; P for perpendicular. The blue arrow denotes the shock direction.

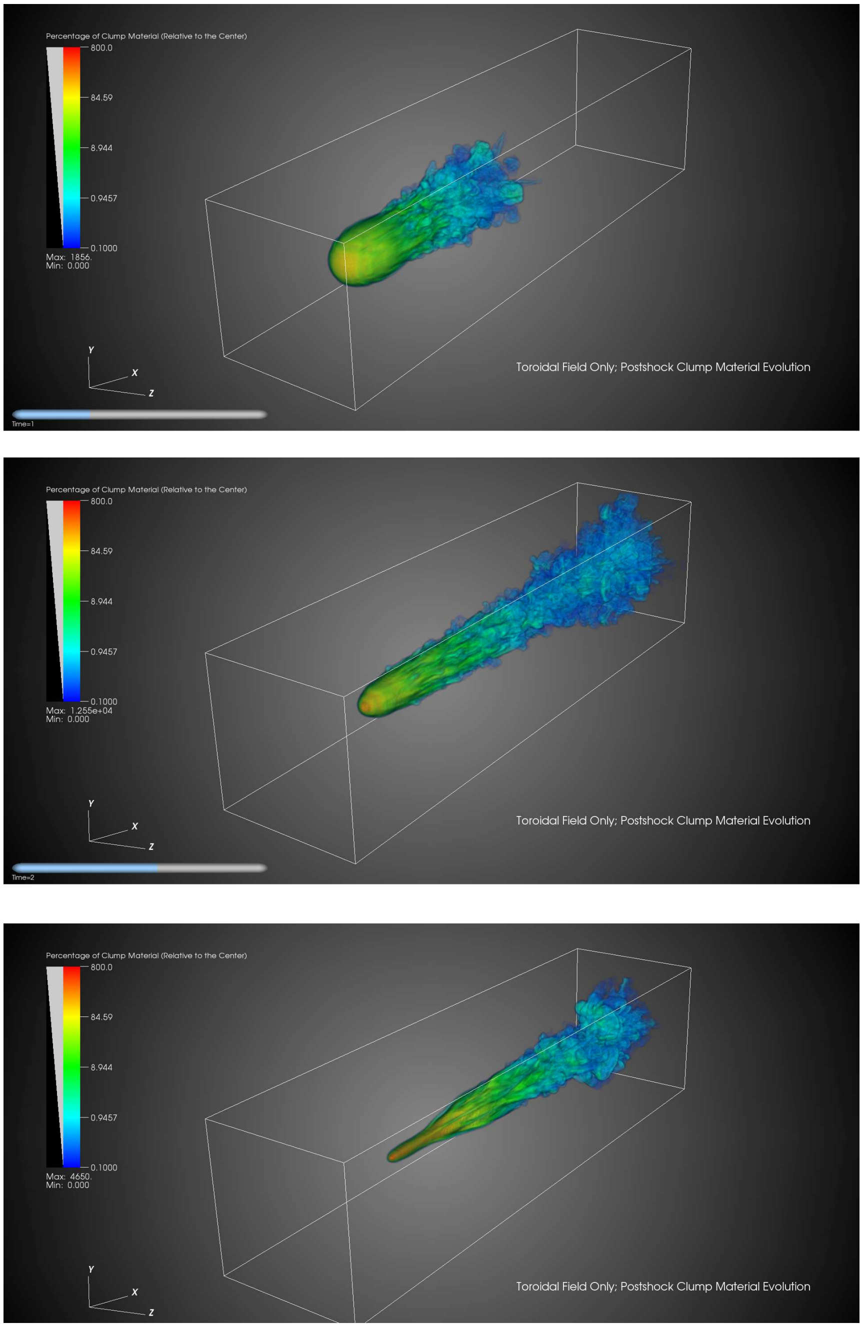

Fig. 4.— Case of toroidal only, aligned with shock propagation direction. Evolution of clump material at 1, 2 and 3.5 clump crushing time. The color indicates clump material concentration, normalized by initial value.

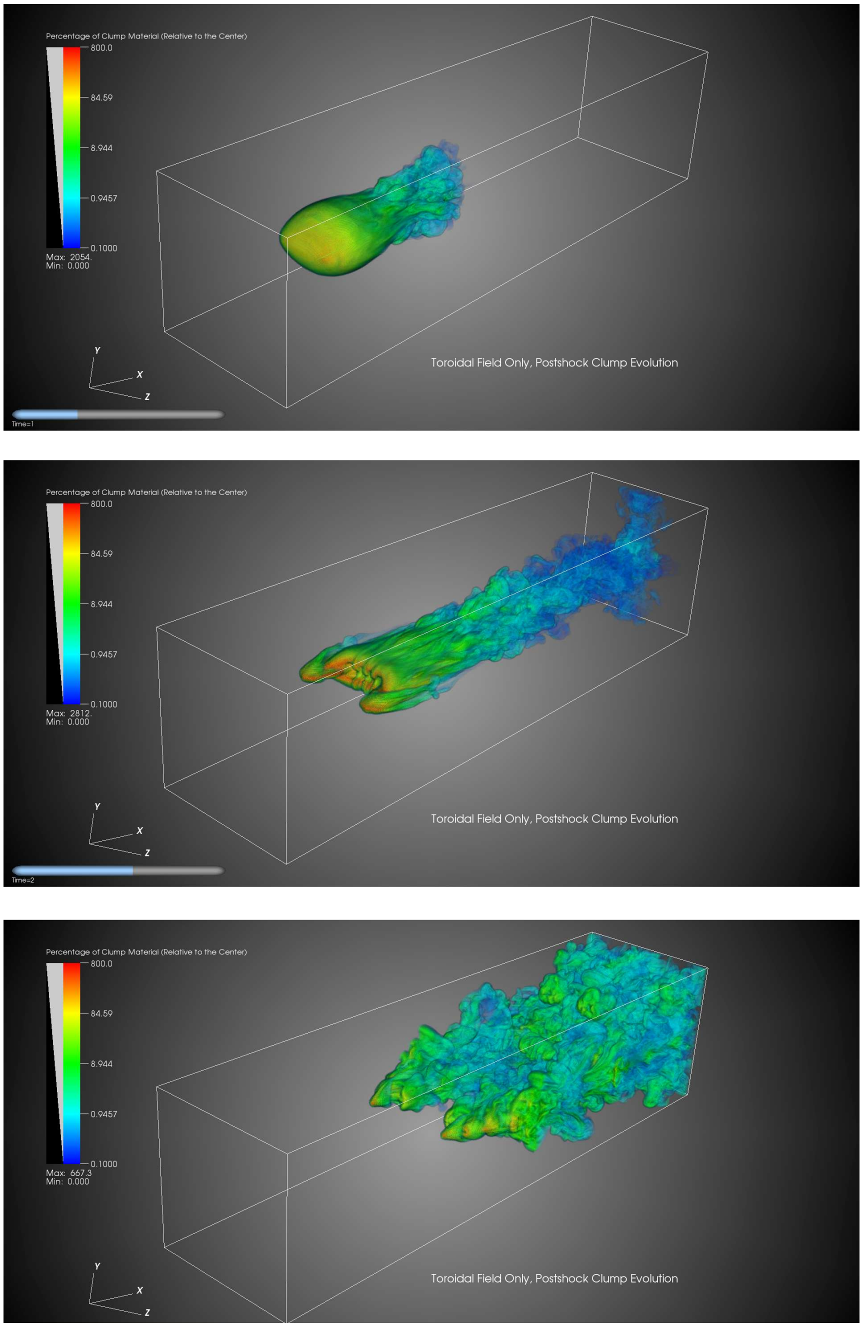

Fig. 5.— Case of toroidal only, perpendicular to shock propagation direction. Evolution of clump material at 1, 2 and 3.5 clump crushing time. The color indicates clump material concentration, normalized by initial value.

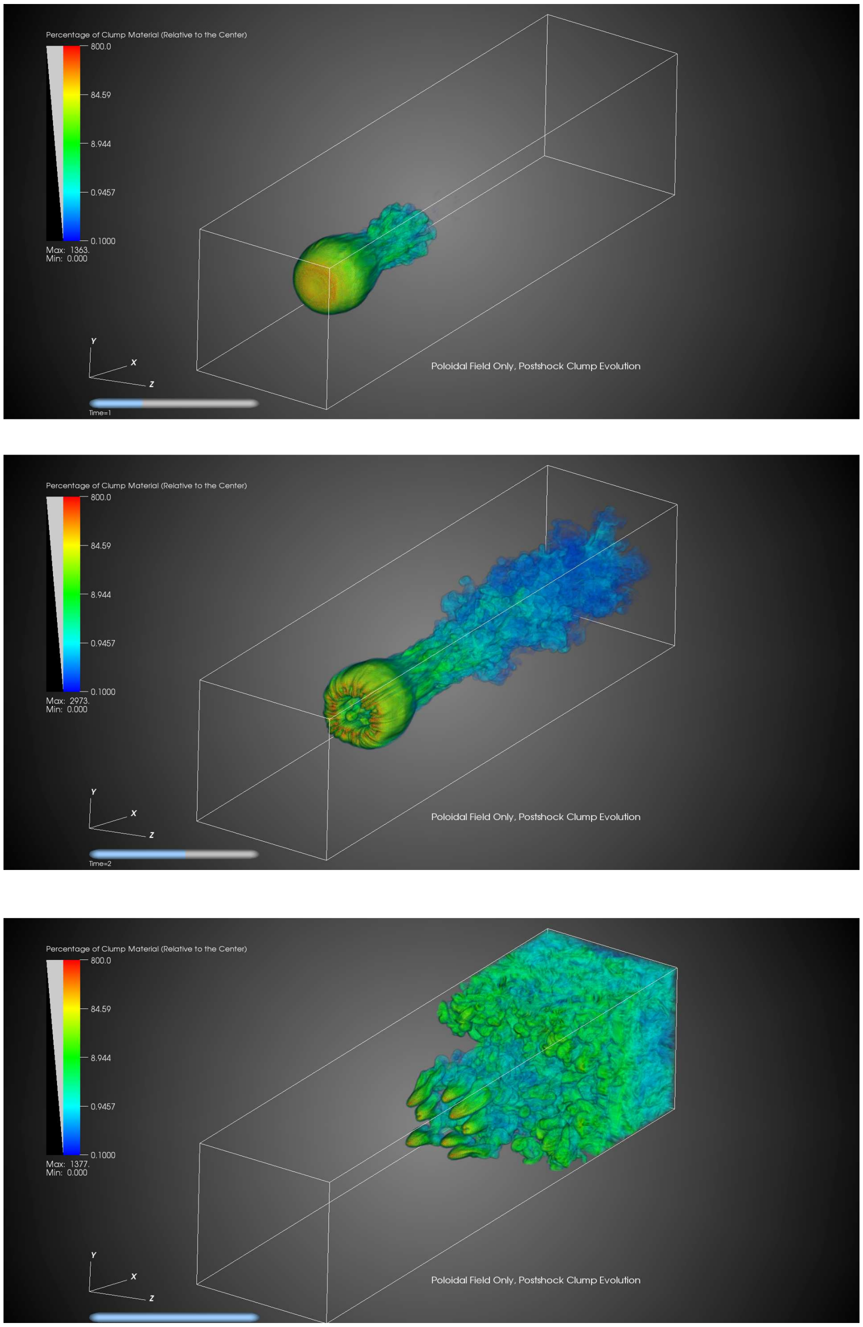

Fig. 6.— Case of poloidal only, aligned with shock propagation direction. Evolution of clump material at 1, 2 and 3.5 clump crushing time. The color indicates clump material concentration, normalized by initial value.

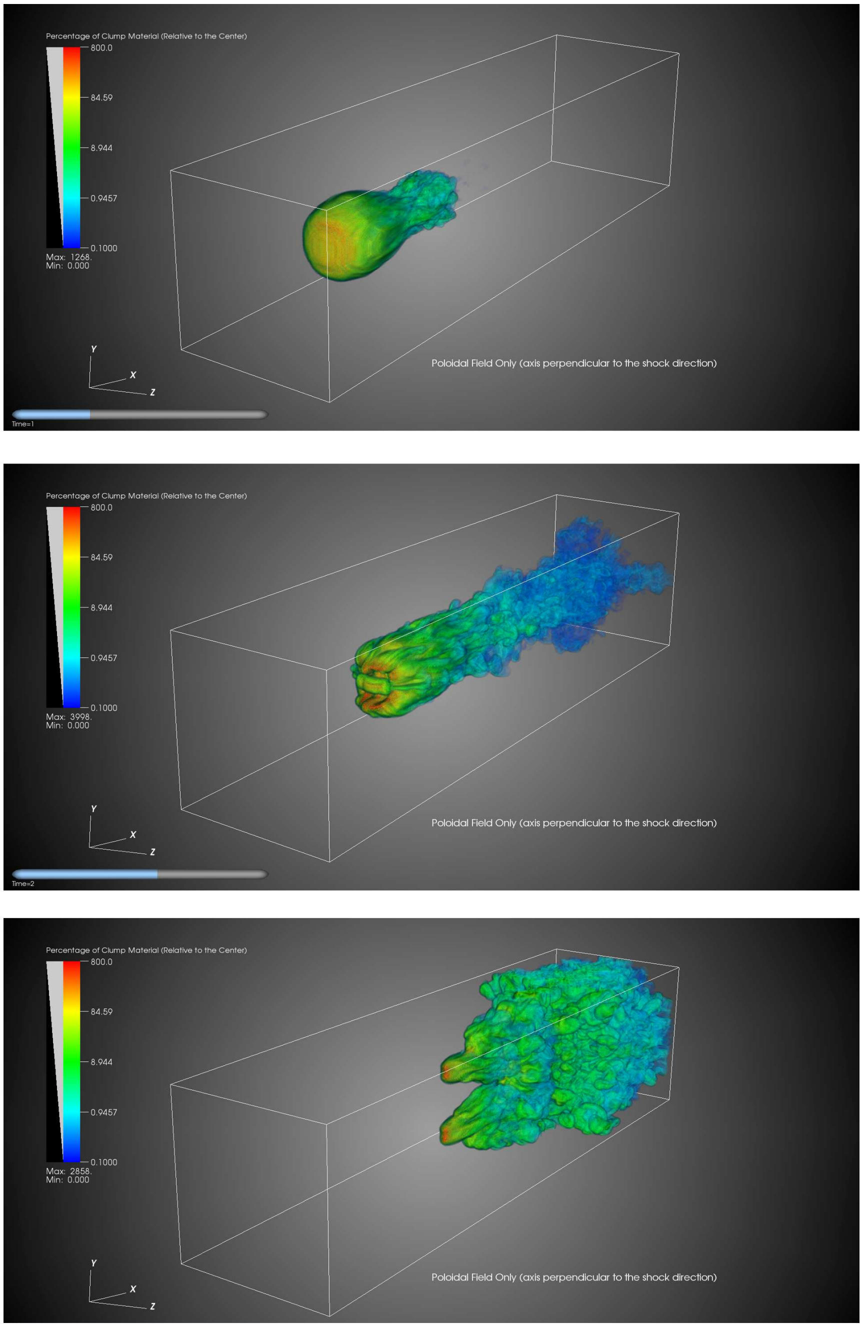

Fig. 7.— Case of poloidal only, perpendicular to shock propagation direction. Evolution of clump material at 1, 2 and 3.5 clump crushing time. The color indicates clump material concentration, normalized by initial value.

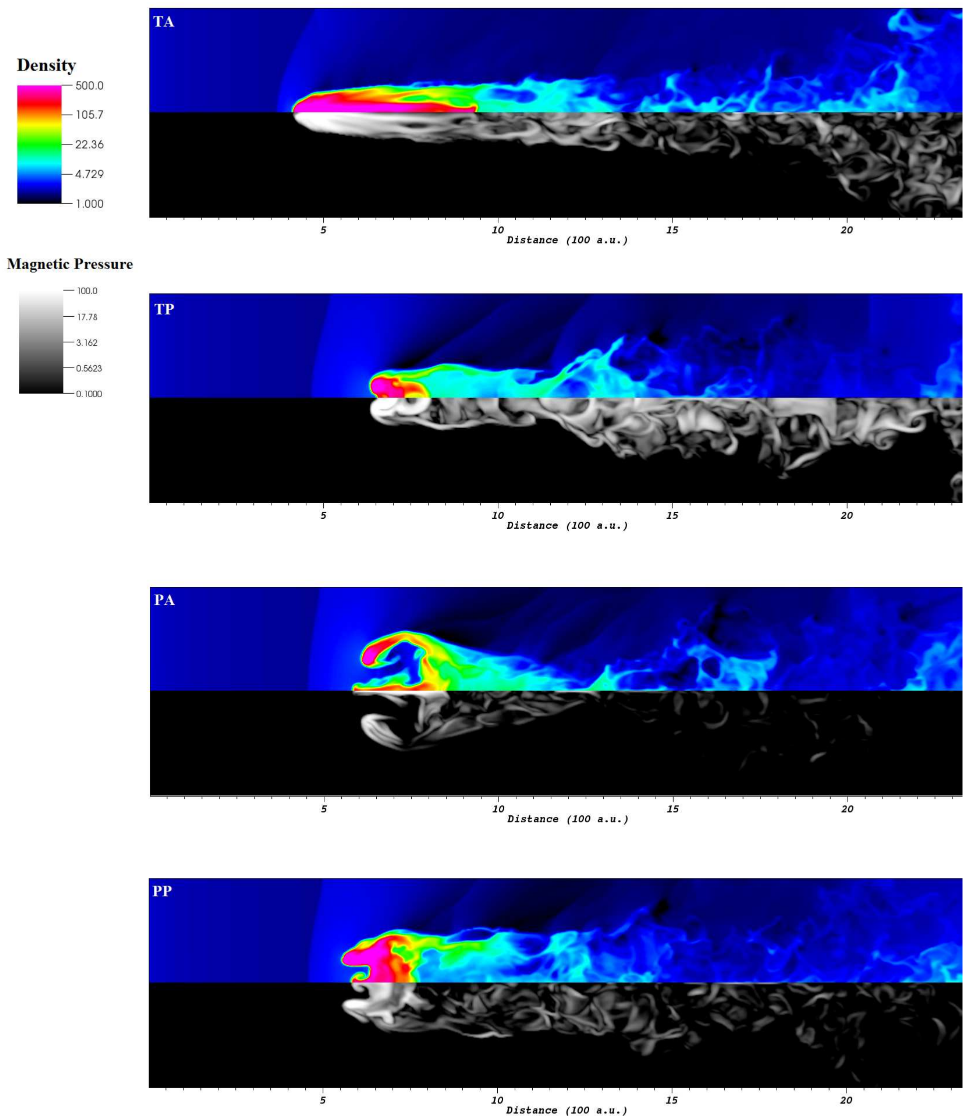

Fig. 8.— Snapshot of shocked clumps cutthrough the center of the domain, at $t = 2\tau_{cc}$. The four panels correspond to the TA, TP, PA, PP cases from top to bottom, respectively. The upper half part of each panel shows the clump density, the lower half part shows the magnetic pressure in pseudocolor.

Table 1: Simulation Setups

Code	β_{avg}	Field Configuration	Field Orientation (related to shock)
TA	0.1	*toroidal*	aligned
TP	0.1	*toroidal*	perpendicular
PA	1	*poloidal*	aligned
PP	1	*poloidal*	perpendicular